



Water limitation regulates positive feedback of increased ecosystem respiration

Received: 14 September 2023

Accepted: 8 July 2024

Published online: 07 August 2024

 Check for updates

Qin Zhang ^{1,2}, Chuixiang Yi ^{3,4,5}✉, Georgia Destouni ^{2,6}, Georg Wohlfahrt ³, Yakov Kuzyakov^{7,8}, Runze Li ⁹, Eric Kutter¹⁰, Deliang Chen ¹¹, Max Rietkerk¹², Stefano Manzoni ², Zhenkun Tian ¹³, George Hendrey^{4,5}, Wei Fang¹⁴, Nir Krakauer ^{5,15}, Gustaf Hugelius ^{2,16}, Jerker Jarsjo ², Jianxu Han^{1,2} & Shiguo Xu¹

Terrestrial ecosystem respiration increases exponentially with temperature, constituting a positive feedback loop accelerating global warming. However, the response of ecosystem respiration to temperature strongly depends on water availability, yet where and when the water effects are important, is presently poorly constrained, introducing uncertainties in climate–carbon cycle feedback projections. Here, we disentangle the effects of temperature and precipitation (a proxy for water availability) on ecosystem respiration by analysing eddy covariance CO₂ flux measurements across 212 globally distributed sites. We reveal a threshold precipitation function, determined by the balance between precipitation and ecosystem water demand, which separates temperature-limited and water-limited respiration. Respiration is temperature limited for precipitation above that threshold function, whereas in drier areas water limitation reduces the temperature sensitivity of respiration and its positive feedback to global warming. If the trend of expansion of water-limited areas with warming climate over the last decades continues, the positive feedback of ecosystem respiration is likely to be weakened and counteracted by the increasing water limitation.

At present ecosystem respiration (R_e) produces about one order of magnitude higher CO₂ than do anthropogenic emissions¹, although R_e emissions are offset by plant primary production. The R_e increases exponentially with temperature, as typically described by Q_{10} (the factor by which respiration increases per 10 °C increase in temperature) and Arrhenius models^{2–4}. These formulations are widely accepted in Earth system models (ESM) and suggest that the carbon transfer rate from soils and plants to the atmosphere will increase with warming, causing positive feedback that further accelerates warming^{5,6}.

Recent observations, however, have led to debates^{7–20} on the extent to which R_e may increase with warming. Uncertainty in the temperature sensitivity of R_e has been attributed mainly to a confounding effect of precipitation^{21,22}. At the ecosystem level, respiration responds to temperature and precipitation through several mechanisms occurring

simultaneously and whose relative importance depends on biomes and climates^{7,20,23}. Models solely driven by temperature can predict R_e well only over a limited temperature range^{8,23,24} and in the absence of water limitation⁷. Recent field studies indicate that precipitation (a proxy for water availability) and supply of accessible substrates (photosynthates for plants or organic matter for decomposers) are confounding factors for the actual feedback of R_e to global warming that may unexpectedly lower the positive feedback in real-world scenarios, depending on local to regional conditions^{7,8,10,23–26}.

Field experiments^{14,19}, modelling studies²⁷ and meta-analyses^{7,8,20} have suggested that R_e responds in different ways to changing hydro-thermal conditions depending on latitude and ecosystem type. The Q_{10} may decrease with increasing temperature^{4,7,8,23,26}, often regulated by water availability¹⁰. However, the temporal and geographic influence

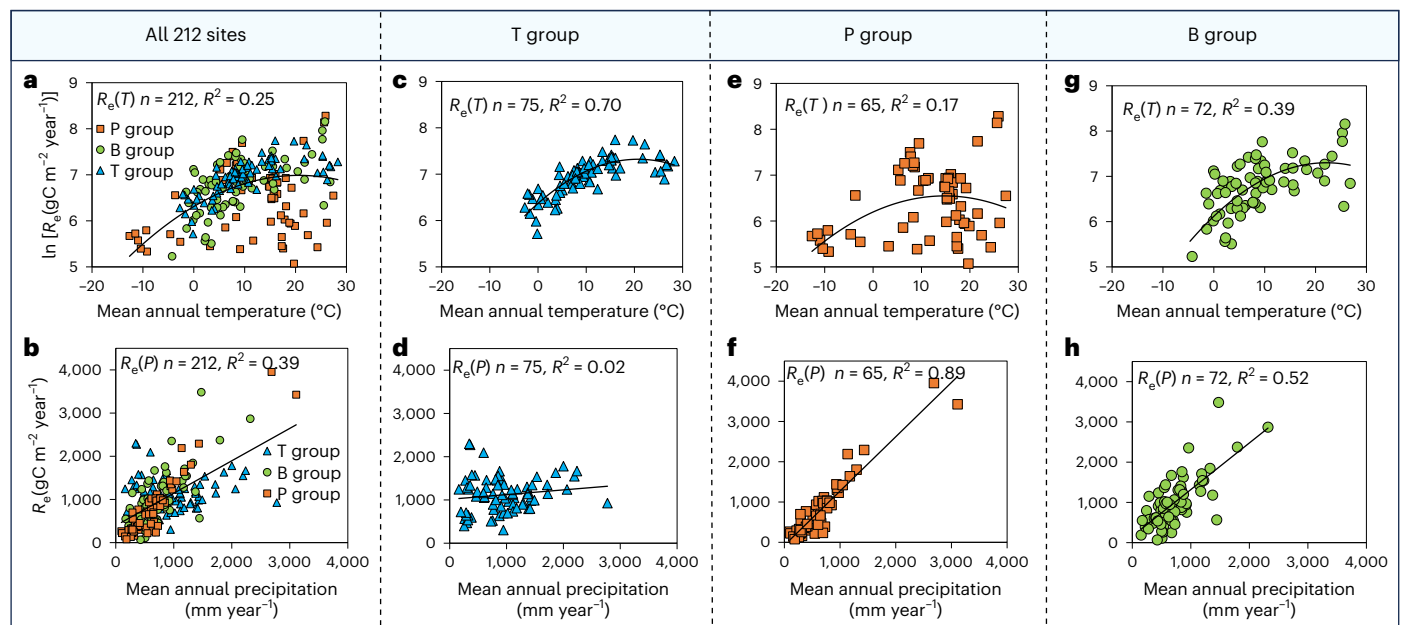


Fig. 1 | The statistical performance of models of ecosystem respiration (R_e) as a function of mean annual temperature (T) and precipitation (P), $R_e(T)$ and $R_e(P)$. **a–h, Models were constructed using: all data for $R_e(T)$ (**a**); all data for $R_e(P)$ (**b**); T group for $R_e(T)$ (**c**); T group for $R_e(P)$ (**d**); P group for $R_e(T)$ (**e**); P group for $R_e(P)$ (**f**); B group for $R_e(T)$ (**g**); and B group for $R_e(P)$ (**h**). Here, the empirical temperature-dependent respiration model $R_e(T)$ refers to equation (11), while**

precipitation-dependent respiration model $R_e(P)$ refers to equation (12). We first calculated site-year average of temperature (T), precipitation (P) and ecosystem respiration R_e across 212 FLUXNET sites. Then we used a mixture regression model (Methods) to statistically classify them into three groups: T group, P group and B group. Finally, we calculated statistics of both empirical models for each group.

of water availability on the temperature sensitivity of R_e remains to be determined. Moreover, the Q_{10} may change under future climate change scenarios⁷. This introduces more—and still poorly understood—complexity to terrestrial carbon budget estimates.

Disentangling the effects of temperature and precipitation on ecosystem R_e is a central challenge for reducing uncertainties in modeling of climate–carbon cycle feedbacks. There is therefore a pressing need to determine where and when the precipitation effects on R_e are important, which is the main research question addressed in this study.

Results

Statistical disentangling

We used statistical models on FLUXNET2015 data²⁸ to examine the effect of mean annual temperature (T) and precipitation (P) on R_e . Despite measurement challenges, FLUXNET2015 provides unique insights. Using a normal mixture regression model, we first identified 32 of the 212 sites of eddy covariance CO_2 flux measurement as temperature limited (prototype T group, with >95% probability of temperature control) and 23 sites as precipitation limited (prototype P group, with >95% probability of precipitation control). Subsequent analyses allowed us to further classify sites into a T group, a P group and a group influenced by both temperature and precipitation (B group), based on relative residuals (Methods and Supplementary Information)

We used an existing empirical temperature-dependent respiration model $R_e(T)$ (equation (10))²⁹ and a precipitation-dependent respiration model $R_e(P)$ (equation (12))^{30,31} to separately fit the data of the T group, P group and B group sites and further verify the effects of temperature and precipitation on R_e obtained from this statistical grouping (Methods and Supplementary Information). Owing to effect combinations, each of the empirical models $R_e(T)$ and $R_e(P)$ could partly explain the observed variability across all data (Fig. 1a,b). However, $R_e(T)$ performed excellently for the T group (Fig. 1c) but poorly for the P group (Fig. 1e), while $R_e(P)$ did poorly for the T group (Fig. 1d) but excellently for the P group (Fig. 1f). The R_e in the B group emerged as dependent on both temperature and precipitation (Fig. 1g,h).

This analysis shows that the grouping was effective in separating ecosystems that are predominantly limited by precipitation (where $R_e(P)$ performs well) or temperature (where $R_e(T)$ performs well). However, these empirical relations do not inform on the combinations of P and T where the transition from P to T limitation occurs, which we need to assess the temperature dependence of R_e under future climates.

Empirical threshold function

We hypothesized that a threshold function exists that separates the biome climate space (T, P) (Fig. 2a) into two distinct regions with: (1) R_e more limited by T ; and (2) R_e more limited by P .

We also expected the B group to straddle the boundary between the T and P groups, with R_e affected by both T and P . As a first step to test this and estimate the conditions under which R_e switches from T control to P control or vice versa, we used the climate data from the B group sites to obtain an empirical threshold precipitation function \tilde{P} of T ,

$$\tilde{P}(T) = 446 \times 10^{0.042T} \quad (1)$$

where \tilde{P} is mean annual precipitation (mm per year) and T is mean annual temperature ($^{\circ}\text{C}$) (Extended Data Fig. 1).

Theoretical basis of the threshold function

To investigate the theoretical basis of the empirical threshold precipitation function $\tilde{P}(T)$, we note that the surface net radiation R_n (MJ m^{-2} per year) is the sum of the sensible heat flux H (MJ m^{-2} per year) used to heat the air and the latent heat flux λET used to evaporate water from the soil and transpire water from plants. Here ET (mm per year) is evapotranspiration and λ (2.5 MJ kg^{-1}) is the latent heat coefficient. Considering the theoretical limits $H \rightarrow 0, R_n \rightarrow \lambda \text{ET}$ we can find a theoretical maximum potential evapotranspiration $\text{PET} = R_n/\lambda$ assuming the available energy R_n to be completely used for evapotranspiration without being constrained by water supply or atmospheric saturation. Budyko defined a dryness index $\text{DI} = \text{PET}/P$, providing essential

climatological water/energy limitation information in a straightforward way: $DI < 1$ indicates wet (energy-limited) and $DI > 1$ dry (water-limited) conditions³².

This framework can be illustrated in a two-dimensional space spanned by the dryness index DI and evapotranspiration index $EI = AET/P$, where AET is actual evapotranspiration³². In wet ($DI < 1$, $P > PET$) regions, AET is limited by the available energy (R_n) and hence EI is expected to be at or below the line $EI = DI$ ($AET = PET$; Fig. 2b). In dry ($DI > 1$, $P < PET$) regions, AET is limited by the available water, so EI is expected to be at or below the line $EI = 1$ ($AET = P$; Fig. 2b).

The transition from temperature (energy) to precipitation (water) limitation of R_e is expected to occur at conditions that are neither too wet nor too dry. Therefore, we hypothesized the theoretical threshold function corresponding to the empirical function in equation (1) to be given by

$$P^* = PET(T), \text{ corresponding to } DI = 1 \quad (2)$$

Thus, P^* is suggested to depend on temperature because the PET is solely determined by R_n . This threshold precipitation function can be estimated, for example, by the Langbein function^{33,34} $P^* = PET = 325 + 21T + 0.9T^2$, originally derived from data for the eastern United States during 1921–1945 and further used, for example, for global water budget estimation³⁵. Direct comparison finally shows that the empirical threshold precipitation function $\tilde{P}(T)$ derived from FLUXNET2015 data closely agrees with the hypothesized theoretical threshold function P^* determined by $DI = 1$ (Fig. 2c). To summarize, our analysis shows that ecosystem respiration is limited by energy (and thus temperature dependent) when the climate is wet ($P > PET$) and is limited by water (and thus precipitation dependent) when the climate is dry ($P < PET$).

Discussion

The effects of temperature and precipitation on R_e can be disentangled empirically and mechanistically (Fig. 2). The condition $DI = 1$ provides function $P^* = PET(T)$ above which R_e is sensitive to T . As DI increases, respiration shifts from being temperature limited to being water limited (Fig. 2b). We used the FLUXNET2015 data of R_e to fit the Q_{10} model for the DI conditions of the different sites (Methods) and obtained apparent Q_{10} at the ecosystem level (Extended Data Figs. 2–4). In wet conditions, the apparent Q_{10} is high and decreases linearly with increasing dryness index ($DI < 1$), while it is low and near-constant in water-limited conditions ($DI > 1$) (Extended Data Fig. 2). The slope of the linear decrease of Q_{10} with temperature (the T sensitivity of Q_{10}) is 3.7 times steeper when $DI < 1$ than when $DI > 1$ (Extended Data Fig. 3). Under the latter, dry conditions, the low substrate supply associated with the water (precipitation) limitation, reduces the biomass of both primary producers and consumers and thereby also reduces enzyme activities and capacity³⁶. In fact, there is direct evidence of reduced carbon flux exchange between soil or canopy and the atmosphere under dry conditions, as the substrate supply to soil microorganisms

and the CO_2 supply to the leaves are then reduced and both supply processes ultimately reduce R_e (refs. 37,38).

Interannual and intersite variations in R_e are confounded by a range of interlinked environmental factors with varying strengths³⁹. Climatic variation and some non-climatic factors, such as topography, soil type, substrate availability and species composition, may account for those unexplained spatial variations in R_e of the three groups. They may also influence our grouping algorithm and explain why sites with similar

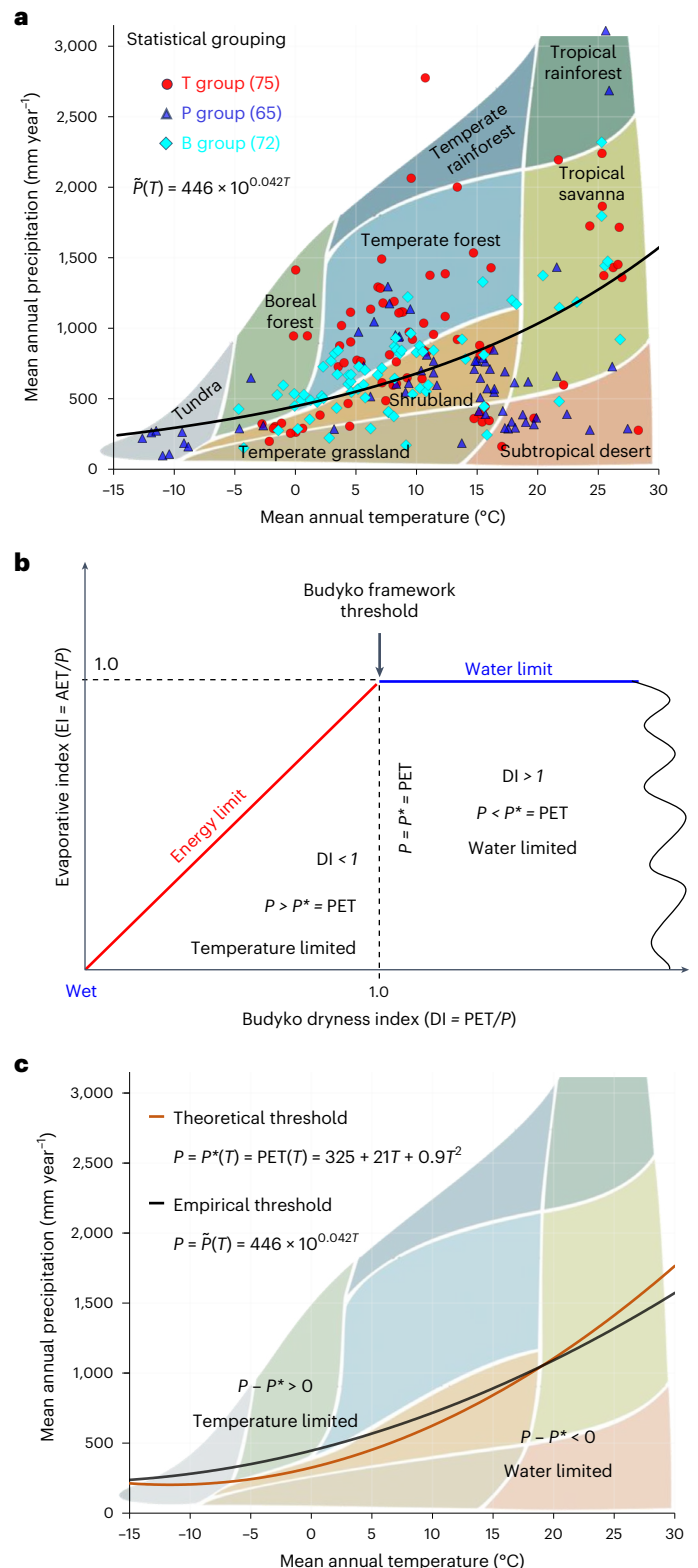


Fig. 2 | Comparative threshold functions for mean temperature (T) or mean precipitation (P) regulation of ecosystem respiration (R_e). **a**, A threshold precipitation function $\tilde{P}(T)$ emerging empirically from grouping of the observational eddy covariance flux data (Methods). **b**, A hypothesized comparative threshold precipitation function $P^*(T) = PET(T)$ determined from the Budyko dryness condition $DI = 1$. **c**, Budyko theoretical threshold and empirical threshold. The empirical function $\tilde{P}(T)$ in **a** was obtained from P and T values at sites belonging to the B group, which are colimited by temperature and precipitation. Then we linked this empirical result to the Budyko framework by assuming that Budyko dryness $DI = 1$ provides the condition to determine a threshold relationship between precipitation with temperature. Thus, the space (T, P) is divided by the threshold curve into two regions—one where R_e is dominated by temperature and one where it is dominated by precipitation.

temperatures and precipitation went to different groups. For instance, tropical rainforests may have been grouped into the P group owing to their low seasonal temperature variability (Fig. 2a). In addition, the correlation between R_e and gross primary production (GPP) is notably higher in the P group than in the T group (Supplementary Fig. 1). This is consistent with studies suggesting that substrate limitation leads to reduced temperature sensitivity.

Recent theoretical studies^{21,40–43} indicate that temperature effects on metabolic fluxes at the ecosystem level can be obtained by integrating the kinetic effects of temperature on the rates of photosynthesis and respiration of individual organisms in the ecosystem. Temperature effects on metabolism at organism level can be described by an expression mathematically equivalent to Arrhenius equation ($\sim \exp(-E_a/kT)$). These effects can be then scaled up to the whole ecosystem by considering the biomass of consumers and primary producers. Many modelling and observational studies have further shown that precipitation is a critical driver for site productivity^{44–47} and many previous studies have reported that Q_{10} is not constant but decreases with increasing temperature^{7,8,23,26,27,48}. In view of these studies, we here introduce and test DI ($= R_n/\lambda P$)^{32,49}, expressing the ratio of available energy to precipitation, as a further quantitative explanatory parameter for both understanding and predicting under which conditions R_e is sensitive to temperature. For instance, precipitation in high-latitude ecosystems can be low, ranging from 150 to 250 mm per year, while the DI is also low because the available energy R_n is even more limited. Therefore, DI is a more informative predictor than T and P alone.

Our conclusions are drawn from broad patterns captured over long timescales across biomes and continents. We acknowledge a potential asymmetric effect of precipitation on R_e , particularly notable in arid and semi-arid ecosystems as a result of seasonal dynamics or spikes in soil respiration triggered by precipitation pulses after prolonged seasonal droughts^{30,50}. Details on the assessment of such second-order effects at subannual timescales are discussed in Extended Data Figs. 5 and 6 and Supplementary Methods 2, while the main focus here is on the first-order effects at the annual timescale.

The temperature insensitivity of R_e under dry conditions indicates a water-availability control and regulation of the positive feedback of R_e to global warming. Expansion of arid areas and contraction of lake and wetland areas have been reported around the world^{51–55}. Output data from climate models also indicate drying of land areas with mean annual temperature >16 °C (ref. 51), while greenhouse gas emissions are expected to continue raising temperatures⁵⁵ with land-surface temperature reported to warm faster (0.27 °C per decade) than sea-surface temperature (0.11 °C per decade) since the 1970s⁵⁶. Continuation of such drying trends under warming can be expected to reduce the positive feedback of R_e to future global warming.

More specifically, our findings indicate that this hydroclimatic trend will change the two main ecosystem carbon fluxes, R_e and GPP, and the balance of CO₂ exchanges between biosphere and atmosphere to weaker associated feedbacks to global warming. By analysing nine ESM outputs from Coupled Model Intercomparison Project Phase 6 (CMIP6), we also found that most models (seven out of nine) failed to reproduce the declining temperature sensitivity of R_e for drier conditions (Supplementary Fig. 3). The observation-based and theoretically/mechanistically supported threshold function between temperature- and precipitation-driven control on respiration rates represents an opportunity to assess if ESMs and land-surface models capture water versus energy limitations correctly and suggest ways to reduce associated model uncertainties in prediction of future climate change.

Methods

FLUXNET2015 data

The FLUXNET2015 dataset (<https://fluxnet.org/data/fluxnet2015-dataset/>) comes from 212 globally distributed eddy covariance sites (over 1,500

site-years) and provides CO₂, water and energy exchange data between terrestrial ecosystem and atmosphere as well as meteorological observations²⁸. This study used annual ecosystem respiration (R_e) from the daytime partitioning method (RECO_DT_VUT_REF, gC m⁻² per year), annual air temperature (TA_F, °C) and annual precipitation (P_F, mm per year) of all the 212 sites. Air temperature (T) is consolidated from data gap-filled using marginal distribution damping method (TA_F_MDS) and downscaled from ERA-Interim reanalysis data product (TA_ERA). Precipitation (P) is consolidated from data measured and downscaled from ERA (P_ERA). Site-average R_e , T and P were averaged using the measurement period of each site. Site-average data rather than site-year data were used for the analyses in this study. In other words, each site contributed only one data point.

Mixture regression model

The grouping method used in this paper is based on mixture regression, which uses the regression function of a response (R_e) on covariates (T and P) to cluster observations^{57,58}. Mixture regression models are thus different from mixture models, which use the population mean to cluster observations^{59–61}. Let $m_1(T)$ and $m_2(P)$ be the regression functions of R_e on T and P , respectively. That is, $m_1(T) = E(R_e | T)$ and $m_2(P) = E(R_e | P)$. In other words, $m_1(T)$ is used to model the regression function of the T group, while $m_2(P)$ is used to model the regression function of the P group. Since most functions can be approximated well by polynomials, we use cubic polynomials to model both $m_1(T)$ and $m_2(P)$,

$$m_1(T) = a_0 + a_1T + a_2T^2 + a_3T^3 \quad (3)$$

and

$$m_2(P) = b_0 + b_1P + b_2P^2 + b_3P^3 \quad (4)$$

Formally, we can describe the mixture regression model in statistical terminology as follows. Let G be a latent group variable and the regression function of R_e on T , P and G ,

$$E(R_e | T, P, G) = m_G(T, P) \quad (5)$$

with $G = 1$ indicating the T group and $G = 2$ indicating the P group and $m_1(T, P) = m_1(T)$ and $m_2(T, P) = m_2(P)$. Since G is a latent group variable, it is not observed. Denote $\pi_1 = p(G = 1)$ and $\pi_2 = p(G = 2)$, the probabilities of an observation belonging to the T and G groups, respectively (with $\pi_1 + \pi_2 = 1$). Thus, this probability quantifies the likelihood that an observation belongs to a particular group. As a result, the probability may provide us a criterion to cluster observations. Further assume the random error ε in the regression model of R_e over T , P and G follows a normal distribution with mean 0 and variance σ^2 . That is,

$$R_e = m_G(T, P) + \varepsilon \quad (6)$$

where $\varepsilon \sim N(0, \sigma^2)$. This enables deriving the likelihood function of the mixture regression models based on a set of observations and finding maximum likelihood values of the model parameters, $a_0, a_1, a_2, a_3, b_0, b_1, b_2, b_3, \pi_1, \pi_2$ and σ^2 . Unlike with simple linear regression, there is no closed-form solution for these values and finding the maximum likelihood is in general challenging. In the literature of mixture regression model^{62,63}, expectation maximization (EM)⁶⁴ algorithm is used to maximize the likelihood function. During the course of an iteration of the EM algorithm, we also obtain the probability $p(G_i = 2, | T_i, P_i)$ for the observation (R_{e_i}, T_i, P_i) for i th site, $k = 1, 2$. This probability can be used to group observations and is also referred to as posterior probability, although there are no specifically Bayesian statistical concepts in this model. Sites whose probabilities do not meet this threshold are clustered into the B group.

Grouping method

The first step in our data analysis is to identify sites in T and P groups with high confidence from the 212 eddy covariance sites. We apply the mixture regression model for the data collected from sites and obtain the posterior probability $p(G_i = 1, | T_i, P_i)$ for the i th site, $i = 1, \dots, 212$ and $k = 1, 2$. We determine the sites with >95% probability of belonging to T group or P group as two prototype subgroups. That is, if $p(G_i = 1, | T_i, P_i) > 95\%$, then the i th site belongs to the T group and if $p(G_i = 2, | T_i, P_i) > 95\%$, then the i th site belongs to the P group. On the basis of this criterion, 32 highly temperature-limited sites (>95% confidence) and 23 highly precipitation-limited sites (>95% confidence) were selected. Then the two prototype equations predict the annual R_e of any sites:

$$R_e^T(T) = m_1(T) = -0.20T^3 + 5.58T^2 + 22.3T + 538 \quad (7)$$

and

$$R_e^P(P) = m_2(P) = -(2.34 \times 10^{-7})P^3 + (7.26 \times 10^{-4})P^2 + 1.16P - 183 \quad (8)$$

The second step in our analysis is to cluster the sites on the basis of the dimensionless residual index⁶⁵. The residual index is defined as:

$$\text{Residual index} = \frac{\varepsilon_P - \varepsilon_T}{\varepsilon_P + \varepsilon_T} \quad (9)$$

where $\varepsilon_P = |(R_e^P - R_e^{EC})/R_e^{EC}| \times 100\%$ is a percentage error in R_e prediction by equation (8) for a site and R_e^{EC} is the semimeasured annual mean R_e of the site. Similarly, $\varepsilon_T = |(R_e^T - R_e^{EC})/R_e^{EC}| \times 100\%$ is a percentage error in R_e prediction by equation (7) for a site. Intuitively, a large positive residual index value indicates that temperature controls the R_e while a large negative residual index value means that precipitation controls R_e of the site. A residual index value of around zero indicates that equations (7) and (8) have similar predictive ability. The R_e of the sites with a residual index near zero appear to be controlled by both temperature and precipitation. On the basis of equations (7), (8) and (9), we calculate the residual index for each site. We further group the 212 global distributed eddy covariance sites into three groups on the basis of their residual index values: temperature-limited group (T group, residual index > 30%); Precipitation-limited group (P group, residual index < -30%); both-limited by temperature and precipitation group (B group, -30% < residual index < 30%). There were a few sites (five) that we discovered were limited by neither temperature nor precipitation. We chose to leave those unusual sites in the B group. While these sites may demonstrate substantial deviations from the threshold function (Extended Data Fig. 1), most sites in the B group exhibit influences from both temperature and precipitation on ecosystem respiration.

We also calculated the residual index using datasets obtained from the daytime partitioning method; the results showed residual index values derived from night time and daytime partitioning methods show a robust agreement, closely following the 1:1 line (Supplementary Fig. 3).

Empirical R_e models

Equations (7) and (8) in polynomial form are essential for our grouping method and we aim for the purely mathematical fitting to be supported by observational evidence. We used the following model²⁹:

$$R_e(T) = ae^{bT+cT^2} \quad (10)$$

as an empirical temperature-control model of ecosystem respiration. For convenience, we rewrote the equation (10) into a quadratic expression after log-transformation,

$$\ln R_e(T) = a' + b \times T + c \times T^2 \quad (11)$$

The statistical performances of $R_e(T)$ with temperature for all data, T group, P group and B group are shown in Fig. 2a,c,e,g, respectively. The R_e -precipitation relationship is often described by a linear model with long-term site-based data^{30,31},

$$R_e(P) = a_1 \times P - b_1 \quad (12)$$

We used equation (12) as an empirical precipitation-control model of ecosystem respiration. The regression results of $R_e(P)$ with precipitation in different data groups are shown in Fig. 2b,d,f,h, respectively.

Apparent Q_{10}

We divided the 212 FLUXNET2015 sites into five groups according to their site-annual mean DI, $0 < DI < 0.4$ (9 sites); $0.4 < DI < 0.7$ (61 sites); $0.7 < DI < 1.0$ (58 sites); $1.0 < DI < 1.4$ (38 sites); $1.4 < DI < 2.2$ (23 sites); and $DI > 2.2$ (23 sites). The DI is defined as,

$$DI = \frac{P^*(T)}{P} \quad (13)$$

where $P^*(T)$ is the threshold precipitation defined by equation (2) (Fig. 2c) and P is site mean annual precipitation (mm per year).

We estimated the apparent Q_{10} for each of the five groups through the van't Hoff Q_{10} model³,

$$R_e = \alpha e^{\beta T}, Q_{10} = e^{\beta 10} \quad (14)$$

where R_e is site-annual ecosystem respiration, T is site mean annual temperature in °C, α and β are regression parameters. Q_{10} (temperature sensitivity) is the factor of 10 °C increase in temperature multiplied by the R_e .

Reporting summary

Further information on research design is available in the Nature Portfolio Reporting Summary linked to this article.

Data availability

All data used for this study are publicly accessible and downloadable and all results of this study can be reproduced according to the methods provided. The FLUXNET2015 dataset used here are publicly available at <https://fluxnet.org/data/fluxnet2015-dataset/>. The CMIP6 data are publicly available at <https://esgf-node.lnl.gov/projects/cmip6/>. Information on the 212 sites used in this paper and their groupings are available on GitHub (<https://github.com/chuixiangyi/Water-limitation>).

Code availability

The Matlab code used for the analysis is available on GitHub (<https://github.com/chuixiangyi/>).

References

1. The Intergovernmental Panel on Climate Change. *Climate Change 2021: The Physical Science Basis* (eds Masson-Delmotte, V. et al.) (Cambridge Univ. Press, 2021).
2. Lloyd, J. & Taylor, J. On the temperature dependence of soil respiration. *Funct. Ecol.* **8**, 315–323 (1994).
3. van't Hoff, J. H. *Lectures on Theoretical and Physical Chemistry; Part 1 Chemical Dynamics* (Edward Arnold, 1898).
4. Tjoelker, M. G., Oleksyn, J. & Reich, P. B. Modelling respiration of vegetation: evidence for a temperature-dependent Q_{10} . *Glob. Change Biol.* **7**, 223–330 (2001).
5. Cox, P. M., Betts, R. A., Jones, C. D., Spall, S. A. & Totterdell, I. J. Acceleration of global warming due to carbon-cycle feedbacks in a coupled climate model. *Nature* **408**, 184–187 (2000).

6. Barford, C. C. et al. Factors controlling long- and short-term sequestration of atmospheric CO₂ in a mid-latitude forest. *Science* **294**, 1688–1691 (2001).
7. Niu, B. et al. Warming homogenizes apparent temperature sensitivity of ecosystem respiration. *Sci. Adv.* **7**, 15 (2021).
8. Johnston, A. S. A. et al. Temperature thresholds of ecosystem respiration at a global scale. *Nat. Ecol. Evol.* **5**, 487–494 (2021).
9. Crowther, T. W. et al. Quantifying global soil carbon losses in response to warming. *Nature* **540**, 104–108 (2016).
10. Fan, N. et al. Global apparent temperature sensitivity of terrestrial carbon turnover modulated by hydrometeorological factors. *Nat. Geosci.* **15**, 989–994 (2022).
11. Allison, S. D., Wallenstein, M. D. & Bradford, M. A. Soil-carbon response to warming dependent on microbial physiology. *Nat. Geosci.* **3**, 336–340 (2010).
12. Wieder, W. R., Bonan, G. B. & Allison, S. D. Global soil carbon projections are improved by modelling microbial processes. *Nat. Clim. Change* **3**, 909–912 (2013).
13. Tang, J. & Riley, W. J. Weaker soil carbon–climate feedbacks resulting from microbial and abiotic interactions. *Nat. Clim. Change* **5**, 56–60 (2015).
14. Bradford, M. A. et al. Thermal adaptation of soil microbial respiration to elevated temperature. *Ecol. Lett.* **11**, 1316–1327 (2008).
15. Giardina, C. P. & Ryan, M. G. Evidence that decomposition rates of organic matter in mineral soil do not vary with temperature. *Nature* **404**, 858–861 (2000).
16. Davidson, E. A., Trumbore, S. E. & Amundson, R. Soil warming and organic carbon content. *Nature* **408**, 789–790 (2000).
17. Knorr, W., Prentice, I., House, J. & Holland, E. Long-term sensitivity of soil carbon turnover to warming. *Nature* **433**, 298–301 (2005).
18. Bradford, M. A. et al. Managing uncertainty in soil carbon feedbacks to climate change. *Nat. Clim. Change* **6**, 751–758 (2016).
19. Luo, Y., Wan, S., Hui, D. & Wallace, L. L. Acclimatization of soil respiration to warming in a tall grass prairie. *Nature* **413**, 622–625 (2001).
20. Mahecha, M. D. et al. Global convergence in the temperature sensitivity of respiration at ecosystem level. *Science* **329**, 838–840 (2010).
21. Reichstein, M. et al. Modeling temporal and large-scale spatial variability of soil respiration from soil water availability, temperature and vegetation productivity indices. *Glob. Biogeochem. Cycles* **17**, 15.1–15.15 (2003).
22. Raich, J. W. et al. Potential net primary productivity in South America: application of a global model. *Ecol. Appl.* **1–4**, 399–429 (1991).
23. Davidson, E. A. & Janssens, I. A. Temperature sensitivity of soil carbon decomposition and feedbacks to climate change. *Nature* **440**, 165–173 (2006).
24. Davidson, E. A., Janssens, I. A. & Luo, Y. On the variability of respiration in terrestrial ecosystems: moving beyond Q₁₀. *Glob. Change Biol.* **12**, 154–164 (2006).
25. Yvon-Durocher, G. et al. Reconciling the temperature dependence of respiration across timescales and ecosystem types. *Nature* **487**, 472–476 (2012).
26. Kirschbaum, M. U. F. Soil respiration under prolonged soil warming: are rate reductions caused by acclimation or substrate loss? *Glob. Change Biol.* **10**, 1870–1877 (2004).
27. Atkin, O. K. & Tjoelker, M. G. Thermal acclimation and the dynamic response of plant respiration to temperature. *Trends Plant Sci.* **8**, 343–351 (2003).
28. Pastorello, G. et al. The FLUXNET2015 dataset and the ONEFlux processing pipeline for eddy covariance data. *Sci. Data* **7**, 225 (2020).
29. Hashimoto, S. et al. Global spatiotemporal distribution of soil respiration modeled using a global database. *Biogeosciences* **12**, 4121–4132 (2015).
30. Du, Y. et al. The response of soil respiration to precipitation change is asymmetric and differs between grasslands and forests. *Glob. Change Biol.* **26**, 6015–6024 (2020).
31. Liu, W., Zhang, Z. & Wan, S. Predominant role of water in regulating soil and microbial respiration and their responses to climate change in a semiarid grassland. *Glob. Change Biol.* **15**, 184–195 (2009).
32. Yi, C. & Jackson, N. A review of measuring ecosystem resilience to disturbance. *Environ. Res. Lett.* **16**, 053008 (2021).
33. Jaramillo, F., Prieto, C., Lyon, S. W. & Destouni, G. Multimethod assessment of evapotranspiration shifts due to non-irrigated agricultural development in Sweden. *J. Hydrol.* **484**, 55–62 (2013).
34. Langbein, W. B. *Annual Runoff in the United States* (USGS, 1949).
35. Jaramillo, F. & Destouni, G. Local flow regulation and irrigation raise global human water consumption and footprint. *Science* **350**, 1248–1251 (2015).
36. Razavi, B. S., Blagodatskaya, E. & Kuzyakov, Y. Nonlinear temperature sensitivity of enzyme kinetics explains canceling effect—a case study on loamy haplic Luvisol. *Front. Microbiol.* **6**, 1126 (2015).
37. Moyano, F. E., Manzoni, S. & Chenu, C. Responses of soil heterotrophic respiration to moisture availability: an exploration of processes and models. *Soil Biol. Biochem.* **59**, 72–85 (2013).
38. Katul, G. G., Oren, R., Manzoni, S., Higgins, C. & Parlange, M. B. Evapotranspiration: a process driving mass transport and energy exchange in the soil–plant–atmosphere–climate system. *Rev. Geophys.* **50**, RG3002 (2012).
39. Zhou, H. et al. Relative importance of climatic variables, soil properties and plant traits to spatial variability in net CO₂ exchange across global forests and grasslands. *Agr. For. Meteorol.* **307**, 108506 (2021).
40. Allen, A. P., Gillooly, J. F. & Brown, J. H. Linking the global carbon cycle to individual metabolism. *Funct. Ecol.* **19**, 202–213 (2005).
41. Enquist, B. J. et al. Scaling metabolism from organisms to ecosystems. *Nature* **423**, 639–642 (2003).
42. German, D. P., Marcelo, K. R., Stone, M. M. & Allison, S. D. The Michaelis–Menten kinetics of soil extracellular enzymes in response to temperature: a cross-latitudinal study. *Glob. Change Biol.* **18**, 1468–1479 (2012).
43. Stone, M. M. et al. Temperature sensitivity of soil enzyme kinetics under N-fertilization in two temperate forests. *Glob. Change Biol.* **18**, 1173–1184 (2012).
44. Lieth, H. in *Primary Productivity of the Biosphere* (eds Lieth, H. & Whittaker, R. H.) 237–263 (Springer-Verlag, 1975).
45. Field, C. B., Behrenfeld, M. J., Randerson, J. T. & Falkowski, P. Primary production of the biosphere: integrating terrestrial and oceanic components. *Science* **281**, 237–240 (1998).
46. Cavicchioli, R. et al. Scientists’ warning to humanity: microorganisms and climate change. *Nat. Rev. Microbiol.* **17**, 569–586 (2019).
47. Wei, S. et al. Data-based perfect-deficit approach to understanding climate extremes and forest carbon assimilation capacity. *Environ. Res. Lett.* **9**, 065002 (2014).
48. Kirschbaum, M. U. F. The temperature dependence of soil organic matter decomposition, and the effect of global warming on soil organic C storage. *Soil Biol. Biochem.* **27**, 753–760 (1995).
49. Orth, R., Destouni, G., Jung, M. & Reichstein, M. Large-scale biospheric drought response intensifies linearly with drought duration in arid regions. *Biogeosciences* **17**, 2647–2656 (2020).
50. Jarvis, P. et al. Drying and wetting of Mediterranean soils stimulates decomposition and carbon dioxide emission: the “Birch effect”. *Tree Physiol.* **27**, 929–940 (2007).

51. Yi, C., Wei, S. & Hendrey, G. Warming climate extends dryness-controlled areas of terrestrial carbon sequestration. *Sci. Rep.* **4**, 5472 (2014).
52. Dai, A. Increasing drought under global warming in observations and models. *Nat. Clim. Change* **3**, 52–58 (2013).
53. Ritchie, P. D., Parry, I., Clarke, J. J., Huntingford, C. & Cox, P. M. Increases in the temperature seasonal cycle indicate long-term drying trends in Amazonia. *Commun. Earth Environ.* **3**, 199 (2022).
54. Yao, F. et al. Satellites reveal widespread decline in global lake water storage. *Science* **380**, 743–749 (2023).
55. The Intergovernmental Panel on Climate Change. *Climate Change 2022: Impacts, Adaptation, and Vulnerability* (eds Pörtner, H.-O. et al.) (Cambridge Univ. Press, 2022).
56. Hansen, J., Sato, M. & Ruedy, R. *Global Temperature in 2021* (Columbia Univ., 2022).
57. Kasahara, H. & Shimotsu, S. Testing the number of components in normal mixture regression models. *J. Am. Stat. Assoc.* **110**, 1632–1645 (2015).
58. Zhu, T. H. & Zhang, H. Hypothesis testing in mixture regression models. *J. R. Stat. Soc. B* **66**, 3–16 (2004).
59. Titterton, D. M., Smith, A. F. M. & Makov, U. E. *Statistical Analysis of Finite Mixture Distributions* (Wiley, 1985).
60. Lindsay, B.G. *Mixture Models: Theory, Geometry, and Applications* (Institute of Statistical Mathematics, 1995).
61. Peel, D. & MacLahlan, G. *Finite Mixture Models* (Wiley, 2000).
62. Huang, M., Li, R. & Wang, S. Nonparametric mixture of regression models. *J. Am. Stat. Assoc.* **108**, 929–941 (2013).
63. Huang, M., Li, R., Wang, H. & Yao, W. Estimating mixture of Gaussian processes by kernel smoothing. *J. Bus. Econ. Stat.* **32**, 259–270 (2014).
64. Dempster, A. P., Laird, N. M. & Rubin, D. B. Maximum likelihood from incomplete data via the EM algorithm (with discussion). *J. R. Stat. Soc. B* **39**, 1–38 (1977).
65. Yi, C. et al. Climate control of terrestrial carbon exchange across biomes and continents. *Environ. Res. Lett.* **5**, 034007 (2010).

Acknowledgements

This work used eddy covariance data acquired and shared by the FLUXNET community, including these networks: AmeriFlux, AfriFlux, AsiaFlux, CarboAfrica, CarboEuropeIP, CarboItaly, CarboMont, ChinaFlux, Fluxnet-Canada, GreenGrass, ICOS, KoFlux, LBA, NECC, OzFlux-TERN, TCOS-Siberia and USCCC. The FLUXNET eddy covariance data processing and harmonization were carried out by the ICOS Ecosystem Thematic Center, AmeriFlux Management Project and Fluxdata project of FLUXNET, with the support of CDIAC and the OzFlux, ChinaFlux and AsiaFlux offices. C.Y. completed this research when he was a Fulbright Visiting Professor at University of Innsbruck with support from the US-Austria Fulbright Program. D.C. is supported by the Swedish national strategic research area BECC. G.D. has received support for this research from the Swedish Research Council (VR; grant number 2022-04672). The research of M.R. is supported by

the European Research Council (ERC-Synergy project RESILIENCE, proposal no. 101071417) and by the Dutch Research Council (NWO ‘Resilience in complex systems through adaptive spatial pattern formation’, project no. OCENW.M20.169). S.M. was supported by ERC grant 101001608. G.W. acknowledges support from Austrian Research Promotion Agency grant 878893 and the Austrian Science Fund (10.55776/PAT2661823). N.K. acknowledges funding from National Oceanic and Atmospheric Administration Educational Partnership Program with Minority-Serving Institutions—Cooperative Science Center for Earth System Sciences and Remote Sensing Technologies cooperative agreement grant NA22SEC4810016.

Author contributions

C.Y., Q.Z. and G.D. conceived the project. Q.Z. performed data processing with R.L., Z.T. and J.H. Q.Z. and C.Y. conducted data analysis. C.Y. wrote the first version of the manuscript with Q.Z., E.K., R.L., D.C., G.W., Y.K., G.D., S.M., M.R., G.H. and W.F. All authors discussed the results and contributed to the writing and to the final manuscript.

Competing interests

The authors declare no competing interests.

Additional information

Extended data is available for this paper at <https://doi.org/10.1038/s41559-024-02501-w>.

Supplementary information The online version contains supplementary material available at <https://doi.org/10.1038/s41559-024-02501-w>.

Correspondence and requests for materials should be addressed to Chuixiang Yi.

Peer review information *Nature Ecology & Evolution* thanks Jingfeng Xiao and the other, anonymous, reviewer(s) for their contribution to the peer review of this work. Peer reviewer reports are available.

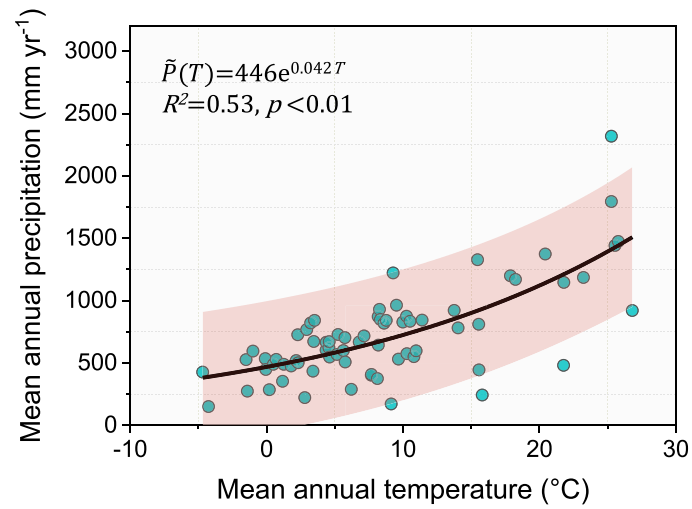
Reprints and permissions information is available at www.nature.com/reprints.

Publisher’s note Springer Nature remains neutral with regard to jurisdictional claims in published maps and institutional affiliations.

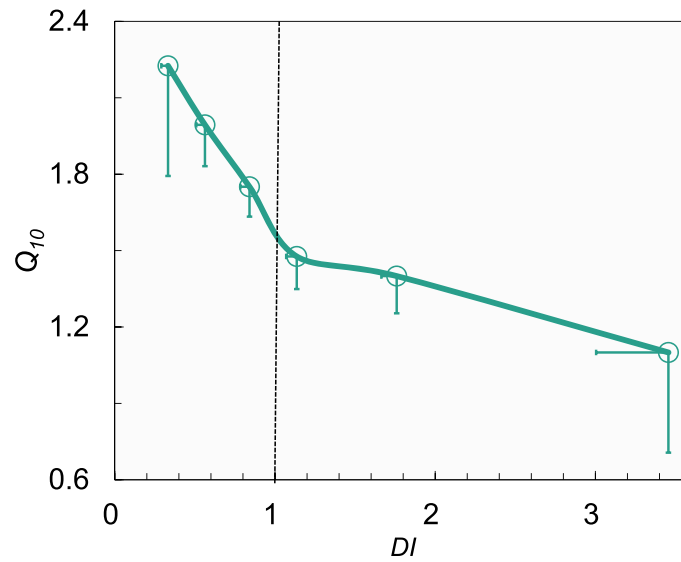
Springer Nature or its licensor (e.g. a society or other partner) holds exclusive rights to this article under a publishing agreement with the author(s) or other rightsholder(s); author self-archiving of the accepted manuscript version of this article is solely governed by the terms of such publishing agreement and applicable law.

© The Author(s), under exclusive licence to Springer Nature Limited 2024

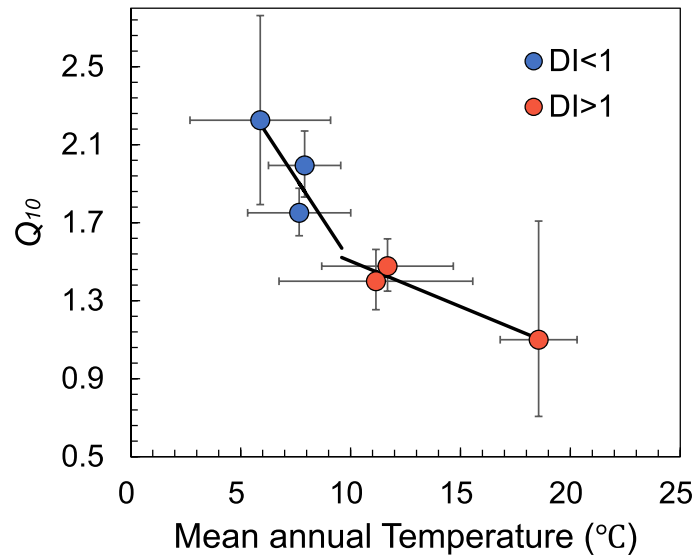
¹Institution of Water and Environment Research, Dalian University of Technology, Dalian, China. ²Department of Physical Geography, Stockholm University, Stockholm, Sweden. ³Universität Innsbruck, Institut für Ökologie, Innsbruck, Austria. ⁴School of Earth and Environmental Sciences, Queens College, City University of New York, Flushing, NY, USA. ⁵Earth and Environmental Sciences Department, Graduate Center, City University of New York, New York, NY, USA. ⁶Department of Sustainable Development, Environmental Science and Engineering, KTH Royal Institute of Technology, Stockholm, Sweden. ⁷Department of Soil Science of Temperate Ecosystems, Department of Agricultural Soil Science, University of Goettingen, Göttingen, Germany. ⁸Peoples Friendship University of Russia (RUDN University), Moscow, Russia. ⁹Department of Statistics, Pennsylvania State University, University Park, PA, USA. ¹⁰Barry Commoner Center for Health & the Environment, Queens College, City University of New York, Flushing, NY, USA. ¹¹Department of Earth Sciences, University of Gothenburg, Gothenburg, Sweden. ¹²Copernicus Institute of Sustainable Development, Utrecht University, TC Utrecht, the Netherlands. ¹³Department of Mathematics and Computer, China University of Labor Relations, Beijing, China. ¹⁴Department of Biology, Pace University, New York, NY, USA. ¹⁵Department of Civil Engineering, The City College of New York, City University of New York, New York, NY, USA. ¹⁶Bolin Centre for Climate Research, Stockholm University, Stockholm, Sweden. ✉e-mail: cyi@qc.cuny.edu



Extended Data Fig. 1 | The statistics of the empirical threshold model $\tilde{P}(T)$. The blue filled circles are the data of mean annual temperature and mean annual precipitation in B-group. The threshold curve (black line) is the exponential regression line with 95% confidence interval (shaded area), $R^2 = 0.53$ and $p < 0.01$ for One-Tailed Test.

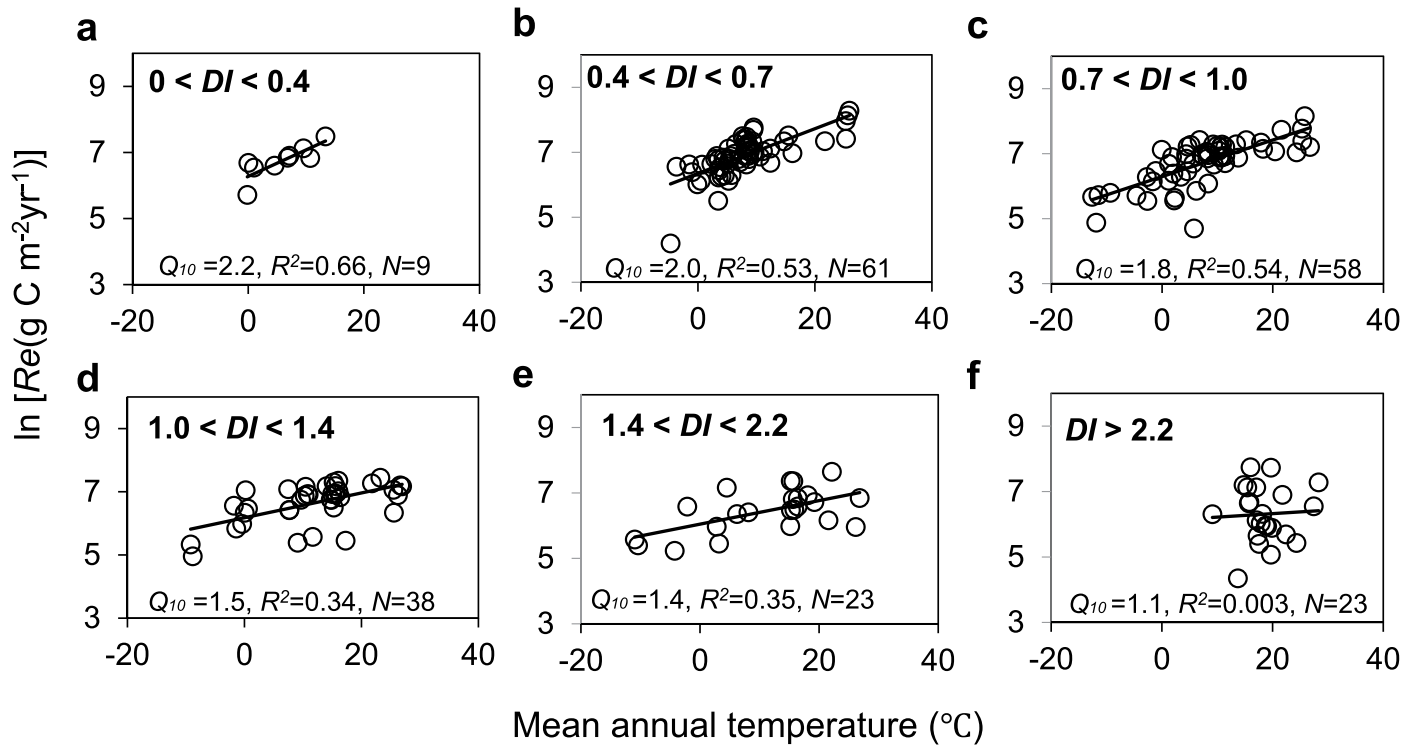


Extended Data Fig. 2 | Differential sensitivity of Q_{10} to Dryness (DI). 212 sites of FLUXNET2015 were divided into six groups with six DI intervals: $0 < DI < 0.4$ (9 sites); $0.4 < DI < 0.7$ (61 sites); $0.7 < DI < 1.0$ (58 sites); $1.0 < DI < 1.4$ (38 sites); $1.4 < DI < 2.2$ (23 sites); and $DI > 2.2$ (23 sites). The apparent group average Q_{10} were estimated by Q_{10} models (see Methods).



Extended Data Fig. 3 | Differential sensitivity of Q_{10} to temperature revealed by Dryness (DI). 212 sites of FLUXNET2015 were divided into six groups with six DI intervals: $0 < DI < 0.4$ (9 sites); $0.4 < DI < 0.7$ (61 sites); $0.7 < DI < 1.0$ (58 sites); $1.0 < DI < 1.4$ (38 sites); $1.4 < DI < 2.2$ (23 sites); and $DI > 2.2$ (23 sites). The filled

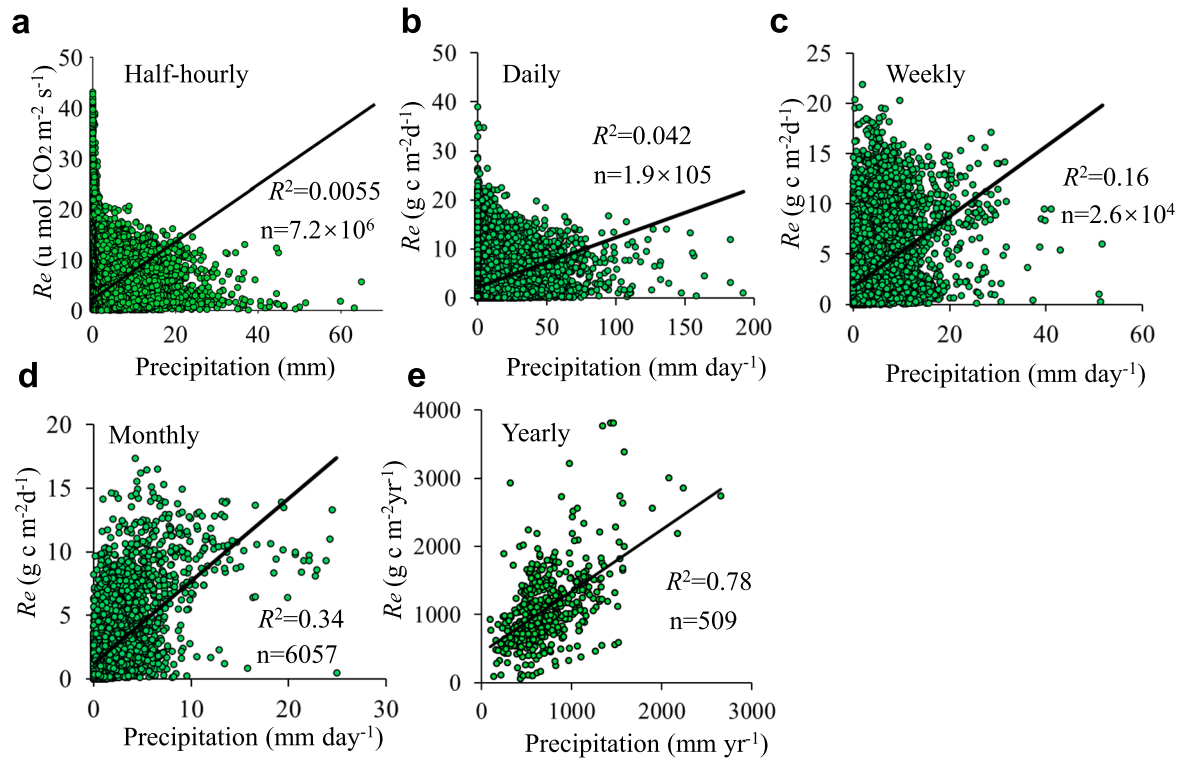
circles and error bars represent DI -group means and their standard deviations, respectively. The blue line is the regression ($y = -0.1719x + 3.2197$, $R^2 = 0.63$ for the data $DI < 1$, while the red line is the regression ($y = -0.047x + 1.97$, $R^2 = 0.93$) for the data $DI > 1$.



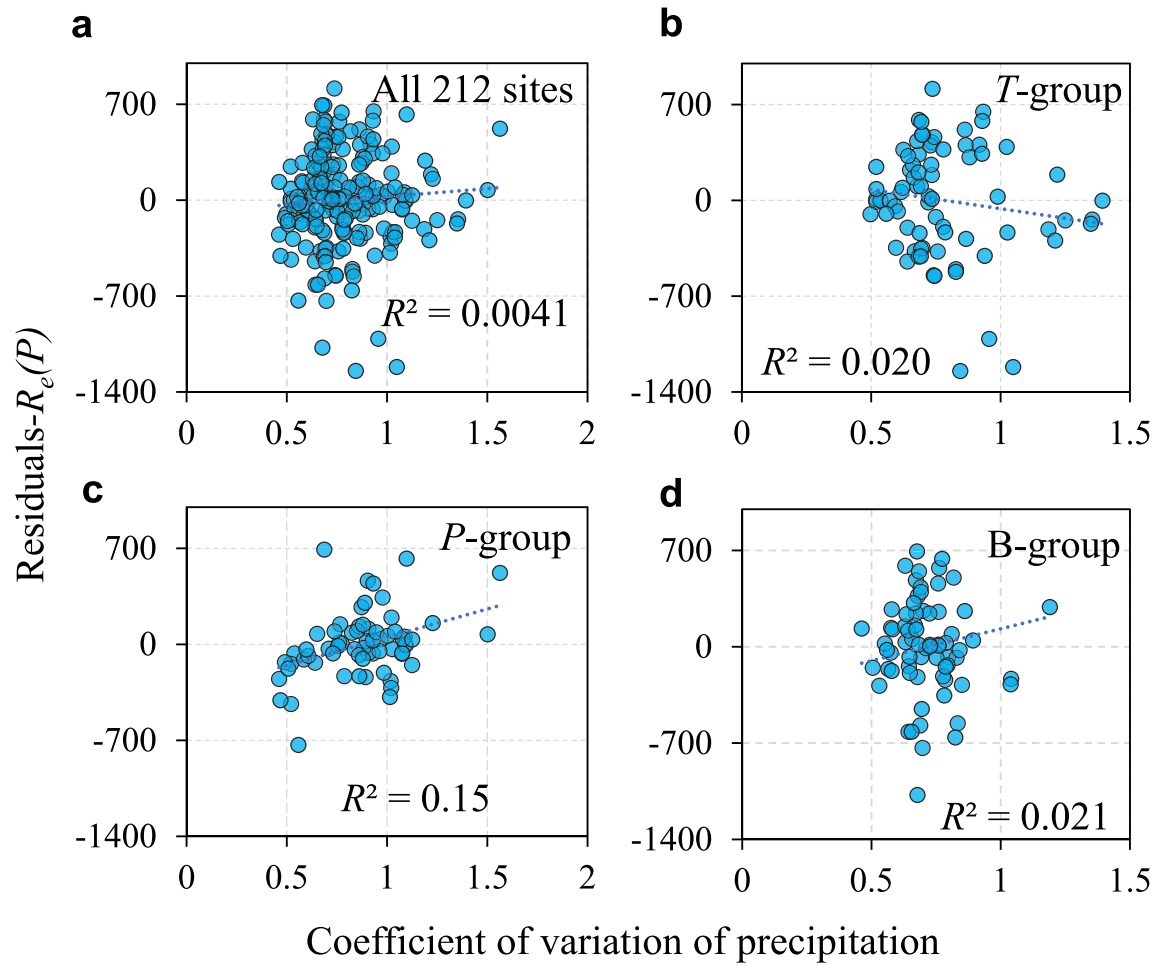
Extended Data Fig. 4 | The distribution and statistics of Q_{10} for each DI group.

212 sites of FLUXNET2015 were divided into six groups with six DI intervals: (a) $0 < DI < 0.4$ (9 sites); (b) $0.4 < DI < 0.7$ (61 sites); (c) $0.7 < DI < 1.0$ (58 sites);

(d) $1.0 < DI < 1.4$ (38 sites); (e) $1.4 < DI < 2.2$ (23 sites); and (f) $DI > 2.2$ (23 sites). Q_{10} was calculated with Q_{10} model (equation (14)) based on FLUXNET2015 ecosystem respiration R_e^{EC} data and temperature data (see Methods).



Extended Data Fig. 5 | The impact of precipitation (P) on ecosystem respiration (R_e) across various time scales based on the data of R_e and P from the same P-group sites. (a) half-hourly; (b) daily; (c) weekly; (d) monthly; and (e) yearly. n is the number of scatter points.



Extended Data Fig. 6 | The asymmetric effect of precipitation (P) on ecosystem respiration (R_e). (a) all sites; (b) T-group; (c) P-group; and (d) B-group. The y-axis represents the residuals of model $R_e(P)$ (equation(12)). The x-axis is coefficient of variation of monthly precipitation.

Reporting Summary

Nature Portfolio wishes to improve the reproducibility of the work that we publish. This form provides structure for consistency and transparency in reporting. For further information on Nature Portfolio policies, see our [Editorial Policies](#) and the [Editorial Policy Checklist](#).

Statistics

For all statistical analyses, confirm that the following items are present in the figure legend, table legend, main text, or Methods section.

- | n/a | Confirmed |
|-------------------------------------|--|
| <input type="checkbox"/> | <input checked="" type="checkbox"/> The exact sample size (n) for each experimental group/condition, given as a discrete number and unit of measurement |
| <input checked="" type="checkbox"/> | <input type="checkbox"/> A statement on whether measurements were taken from distinct samples or whether the same sample was measured repeatedly |
| <input checked="" type="checkbox"/> | <input type="checkbox"/> The statistical test(s) used AND whether they are one- or two-sided
<i>Only common tests should be described solely by name; describe more complex techniques in the Methods section.</i> |
| <input type="checkbox"/> | <input checked="" type="checkbox"/> A description of all covariates tested |
| <input type="checkbox"/> | <input checked="" type="checkbox"/> A description of any assumptions or corrections, such as tests of normality and adjustment for multiple comparisons |
| <input type="checkbox"/> | <input checked="" type="checkbox"/> A full description of the statistical parameters including central tendency (e.g. means) or other basic estimates (e.g. regression coefficient) AND variation (e.g. standard deviation) or associated estimates of uncertainty (e.g. confidence intervals) |
| <input type="checkbox"/> | <input checked="" type="checkbox"/> For null hypothesis testing, the test statistic (e.g. F , t , r) with confidence intervals, effect sizes, degrees of freedom and P value noted
<i>Give P values as exact values whenever suitable.</i> |
| <input checked="" type="checkbox"/> | <input type="checkbox"/> For Bayesian analysis, information on the choice of priors and Markov chain Monte Carlo settings |
| <input checked="" type="checkbox"/> | <input type="checkbox"/> For hierarchical and complex designs, identification of the appropriate level for tests and full reporting of outcomes |
| <input type="checkbox"/> | <input checked="" type="checkbox"/> Estimates of effect sizes (e.g. Cohen's d , Pearson's r), indicating how they were calculated |

Our web collection on [statistics for biologists](#) contains articles on many of the points above.

Software and code

Policy information about [availability of computer code](#)

- | | |
|-----------------|---|
| Data collection | We did not use software in data collection. |
| Data analysis | Code used to generate figures and results is archived at : https://github.com/chuixiangyi/Water-limitation
The following software environment is required to run the code:
Matlab >= 2017 |

For manuscripts utilizing custom algorithms or software that are central to the research but not yet described in published literature, software must be made available to editors and reviewers. We strongly encourage code deposition in a community repository (e.g. GitHub). See the Nature Portfolio [guidelines for submitting code & software](#) for further information.

Data

Policy information about [availability of data](#)

All manuscripts must include a [data availability statement](#). This statement should provide the following information, where applicable:

- Accession codes, unique identifiers, or web links for publicly available datasets
- A description of any restrictions on data availability
- For clinical datasets or third party data, please ensure that the statement adheres to our [policy](#)

The FLUXNET2015 Dataset used here are publicly available at <https://fluxnet.org/data/fluxnet2015-dataset/>. The CMIP6 data are publicly available at <https://esgf-node.lnl.gov/projects/cmip6/>. Information on the 212 sites used in this paper and their groupings are available on GitHub (<https://github.com/chuixiangyi/Water->

limitation). All other data that support the plots within this paper and other findings of this study are available from the corresponding author upon reasonable request. Source data are provided with this paper.

Research involving human participants, their data, or biological material

Policy information about studies with [human participants or human data](#). See also policy information about [sex, gender \(identity/presentation\), and sexual orientation](#) and [race, ethnicity and racism](#).

Reporting on sex and gender	N/A
Reporting on race, ethnicity, or other socially relevant groupings	N/A
Population characteristics	N/A
Recruitment	N/A
Ethics oversight	N/A

Note that full information on the approval of the study protocol must also be provided in the manuscript.

Field-specific reporting

Please select the one below that is the best fit for your research. If you are not sure, read the appropriate sections before making your selection.

Life sciences Behavioural & social sciences Ecological, evolutionary & environmental sciences

For a reference copy of the document with all sections, see [nature.com/documents/nr-reporting-summary-flat.pdf](https://www.nature.com/documents/nr-reporting-summary-flat.pdf)

Ecological, evolutionary & environmental sciences study design

All studies must disclose on these points even when the disclosure is negative.

Study description	We disentangle the impacts of temperature and precipitation (a proxy for water availability) on ecosystem respiration by analyzing eddy covariance CO ₂ flux measurements across 212 globally distributed sites and reveal a threshold precipitation function separating temperature-limited and water-limited respiration.
Research sample	212 globally distributed eddy covariance sites (over 1500 site-years) used in this study.
Sampling strategy	We used all available data
Data collection	The FLUXNET2015 Dataset includes data collected at sites from multiple regional flux networks. The preparation of this FLUXNET Dataset has been possible thanks only to the efforts of many scientists and technicians around the world and the coordination among teams from regional networks
Timing and spatial scale	The FLUXNET2015 dataset used in this study comes from 212 globally distributed eddy covariance sites (over 1500 site-years). This study used annual ecosystem respiration (Re), annual air temperature, and annual precipitation of all the 212 sites. For different sites, the periods are different but all spanning the period 1992–2014.
Data exclusions	No data were excluded from the analyses.
Reproducibility	repository.
Randomization	Randomization is not relevant as we examined the effect over the entire study domain
Blinding	Blind is not relevant because the work was not experimental in nature.
Did the study involve field work?	<input type="checkbox"/> Yes <input checked="" type="checkbox"/> No

Reporting for specific materials, systems and methods

We require information from authors about some types of materials, experimental systems and methods used in many studies. Here, indicate whether each material, system or method listed is relevant to your study. If you are not sure if a list item applies to your research, read the appropriate section before selecting a response.

Materials & experimental systems

n/a	Included in the study
<input checked="" type="checkbox"/>	<input type="checkbox"/> Antibodies
<input checked="" type="checkbox"/>	<input type="checkbox"/> Eukaryotic cell lines
<input checked="" type="checkbox"/>	<input type="checkbox"/> Palaeontology and archaeology
<input checked="" type="checkbox"/>	<input type="checkbox"/> Animals and other organisms
<input checked="" type="checkbox"/>	<input type="checkbox"/> Clinical data
<input checked="" type="checkbox"/>	<input type="checkbox"/> Dual use research of concern
<input checked="" type="checkbox"/>	<input type="checkbox"/> Plants

Methods

n/a	Included in the study
<input checked="" type="checkbox"/>	<input type="checkbox"/> ChIP-seq
<input checked="" type="checkbox"/>	<input type="checkbox"/> Flow cytometry
<input checked="" type="checkbox"/>	<input type="checkbox"/> MRI-based neuroimaging